case the first group) can be efficiently reduced by using the proposed algorithm.

B. Application of the Proposed Algorithm to the Linear HIC

Throughout this part, we consider the case in which the linear HIC detector does not converge if the weighting parameter is not used. Thus, we divide users into two groups, that is, $G = 2$, and we use random highly correlated spreading codes as in [6]. However, the total number of groups G could be set to other values different than 2. In the simulation, we are considering a symbol synchronous system with perfect power control. Fig. 4 illustrates the convergence behavior of the linear HIC, where random codes of length 10 and SNR $= 10$ dB are used. The total number of users is 6, and they are divided into two groups ($\overline{u}_1 = 4$ and $\overline{u}_2 = 2$).

Two methods are used to illustrate the convergence behavior of the HIC. In method 1, the weighting factor is adjusted to $(\mu = 2/(\max|\lambda(\overline{S}^{\mathrm{T}}\overline{S})|))$ (as in [6], for the sake of comparison), whereas in method 2 the weighting factor is adjusted to $(\mu = 2/(\max|\lambda(\overline{\mathbf{S}}_1^T\overline{\mathbf{S}}_1)|))$ (which is the new developed upper bound for the maximum eigenvalue of the systems' transition matrix). To estimate an upper bound for the maximum eigenvalue in both methods, we use the Gershgorin theorem. As depicted in Fig. 4, using method 1, the minimum BER is reached in 22 stages and converges to the decorrelator detector in 60 stages; however, when using method 2, the HIC reaches the minimum BER in 15 stages only and converges to the decorrelator in 45 stages. Therefore, the computational complexity is significantly reduced when the proposed algorithm is used. Note here that the minimum BER is obtained before convergence to the decorrelator detector. This is true especially when highly correlated codes are used. For more details, readers could refer to [4]. Similar conclusions could be obtained for the average BER in Fig. 5. Here, we used the following parameters: $M = 5$, $K = 6$, $N = 10$, $G = 2$ ($\overline{u}_1 = 4$ and $\overline{u}_2 = 2$), and perfect power control to evaluate the average BER.

VII. Conclusion

In this paper, we described the linear HIC as a matrix filtering problem and studied the condition of convergence and its convergence properties. We derived a new upper bound for the maximum eigenvalue of the system's transition matrix. A new ordering and grouping algorithm is proposed to force the maximum eigenvalue of the system's transition matrix to be located in group with index one. In order to illustrate the efficiency of the proposed algorithm, we compared the convergence speed as well the average BER of the HIC using two different methods. Simulation results showed that with the use of the new algorithm, the required number of stages to reach the minimum BER is considerably reduced and therefore the computational complexity of the HIC is reduced as well.

References

[1] M. K. Varanasi, "Group detection for synchronous Gaussian code-division multiple-access channels," *IEEE Trans. Inf. Theory*, vol. 41, no. 4, pp. 1083–1096, Jul. 1995.

[2] L. K. Rasmussen, T. J. Lim, and A. L. Johansson, "A matrix-algebraic approach to successive interference cancellation in CDMA," *IEEE Trans. Commun.*, vol. 48, no. 1, pp. 145–151, Jan. 2000.

[3] ——, "One-shot filtering equivalence for linear successive interference cancellation in CDMA," in *Proc. IEEE 47th Vehicular Technology Conf.*, Phoenix, AZ, May 4–7, 1997, vol. 3, pp. 2163–2167.

[4] A. L. Johansson and L. K. Rasmussen, "Linear group-wise successive interference cancellation in CDMA," in *Proc. IEEE 5th Int. Symp. Spread Spectrum Techniques and Applications*, Sun City, South Africa, Sep. 2–4, 1998, vol. 1, pp. 121–126.

[5] S. Sun, L. K. Rasmussen, H. Sugimoto, and T. J. Lim, "A hybrid interference canceller in CDMA," in *Proc. IEEE 5th Int. Symp. Spread Spectrum Techniques and Applications*, Sun City, South Africa, Sep. 2–4, 1998, vol. 1, pp. 150–154.

[6] S. Sun, L. K. Rasmussen, T. J. Lim, and H. Sugimoto, "A matrix-algebraic approach to linear hybrid interference cancellation in CDMA," in *Proc. Int. Conf. Universal Personal Communications (ICUPC)*, Florence, Italy, Oct. 5–9, 1998, vol. 2, pp. 1319–1323.

[7] A. Grant and C. Schlegel, "Convergence of linear interference cancellation multiuser receivers," *IEEE Trans. Commun.*, vol. 49, no. 10, pp. 1824–1834, Oct. 2001.

[8] D. Guo, L. K. Rasmussen, S. Sun, and T. J. Lim, "A matrix-algebraic approach to linear parallel interference cancellation in CDMA," *IEEE Trans. Commun.*, vol. 48, no. 1, pp. 152–161, Jan. 2000.

[9] M. H. Hayes, *Statistical Digital Signal Processing and Modeling*. New York: Wiley, 1996.

Collision Mitigation by Log-Likelihood Ratio (LLR) Conversion in Orthogonal Code-Hopping Multiplexing

Jae Kyun Kwon, Suwon Park, and Dan Keun Sung

***Abstract*—Log-likelihood ratio (LLR) conversion schemes are proposed to mitigate the effect of collisions (or perforations) that occur in orthogonal code-hopping multiplexing (OCHM), which was previously proposed to accommodate more downlink channels than the number of orthogonal codewords. The proposed LLR conversion schemes greatly reduce the required SNR in channel decoding even when the perforation probability is high. The perforation probability in some LLR conversion schemes is estimated and several estimation methods are proposed. An LLR conversion scheme without estimation of the perforation probability is also proposed to avoid accurate estimation. The performance of the proposed schemes is evaluated by simulation in terms of the required E_b/N_0 for a 1% block error rate (BLER).**

***Index Terms*—Demapping, log-likelihood ratio (LLR), orthogonal code-hopping multiplexing (OCHM), perforation.**

I. Introduction

Code division multiple access (CDMA) downlink usually provides synchronous transmission through orthogonal code sets. Since the number of orthogonal codewords is generally limited, only a limited number of users can be assigned to downlink channels at the same time. In recent years, Internet traffic has rapidly increased in wireless domains. Bursty downlink traffic is expected to be dominant

Manuscript received May 13, 2003; revised October 29, 2004, July 3, 2005, August 24, 2005, and September 26, 2005. This work was supported by Korea Research Foundation Grant (KRF-2002-908-D00036). The review of this paper was coordinated by Prof. T. Lok.

J. K. Kwon was with the Korea Advanced Institute of Science and Technology, Daejeon 305-701, Korea. He is now with Electronics and Telecommunications Research Institute, Daejeon 305-350, Korea (e-mail: jackkwon@ieee.org; jack@etri.re.kr).

S. Park was with the Korea Advanced Institute of Science and Technology, Daejeon 305-701, Korea. He is now with the Departmnt of Electronics and Communications Engineering, Kwangwoon Univerity, Seoul 139-701, Korea (e-mail: spark@ieee.org).

D. K. Sung is with the Department of Electrical Engineering and Computer Science, Korea Advanced Institute of Science and Technology, Daejeon 305-701, Korea (e-mail: dksung@ee.kaist.ac.kr).

Digital Object Identifier 10.1109/TVT.2005.863358

in mobile communications in the future. Low-channel activity due to burstiness results in an inefficient use of code channels and a shortage of available channels in the downlink. Orthogonal code-hopping multiplexing (OCHM) [1], [2] has been proposed as a new multiplexing scheme in which each user uses an orthogonal code-hopping pattern from a limited number of orthogonal codewords, maintaining orthogonality symbol by symbol, and related works [3]–[5] are investigated.

On the other hand, several previous studies have analyzed code-hopping schemes for different purposes in spread spectrum systems. Frequency hopping with a robust feature to narrowband interference was applied to code hopping changing spreading codes [6]. Code hopping was also used to average multiuser interference in the uplink by code diversity [7], [8]. It could be exploited to distinguish cells [9].

Our proposed OCHM can accommodate more downlink orthogonal channels than the number of orthogonal codewords through statistical multiplexing. However, it may cause performance degradation due to hopping pattern collisions during statistical multiplexing. When there exist collisions among the hopping patterns of active downlink channels in OCHM, a comparator and controller at the transmitter of a base station (BS) performs one of two operations. First, if at least one channel-encoded data symbol is different from the others, all data symbols colliding at the moment are perforated and are not transmitted. The transmission power during the encoded and perforated data symbol time is 0 for all related channels. Second, if all channel-encoded data symbols are identical, all the data symbols with collisions are transmitted without perforation. This situation yields an E_s/N_0 gain at the receiver, referred to as synergy. A high-perforation probability degrades the performance of channel decoding. Therefore, collision mitigation schemes should be studied. We propose two log-likelihood ratio (LLR) conversion schemes that improve the decoding performance in perforation environments and investigate the estimation for the perforation probability. Finally, we propose an LLR conversion scheme without estimation.

This paper is organized as follows. Two new LLR conversion schemes and the performance are presented in Section II. Estimation schemes of the perforation probability and simulation results are described in Section III and a fixed linear LLR conversion scheme without estimation of the perforation probability is presented in Section IV. Conclusions are presented in Section V.

II. LLR Conversion for BPSK/QPSK

Channel demodulator output in a soft-input decoder is generally demapped and used as an input value for the decoder. When we transmit d and receive y in conventional BPSK/QPSK, the LLR can be expressed as (1) [10]

$$\begin{aligned} L(d|y) &= \log \frac{P(d=+1|y)}{P(d=-1|y)} \\ &= \log \frac{p(y|d=+1)}{p(y|d=-1)} + \log \frac{P(d=+1)}{P(d=-1)} \\ &= L(y|d) + L(d) \\ &= L(y|d), \qquad \text{for equiprobable symbols} \\ &\propto (y+1)^2 - (y-1)^2, \qquad \text{for AWGN channels} \\ &\propto y. \end{aligned} \tag{1}$$

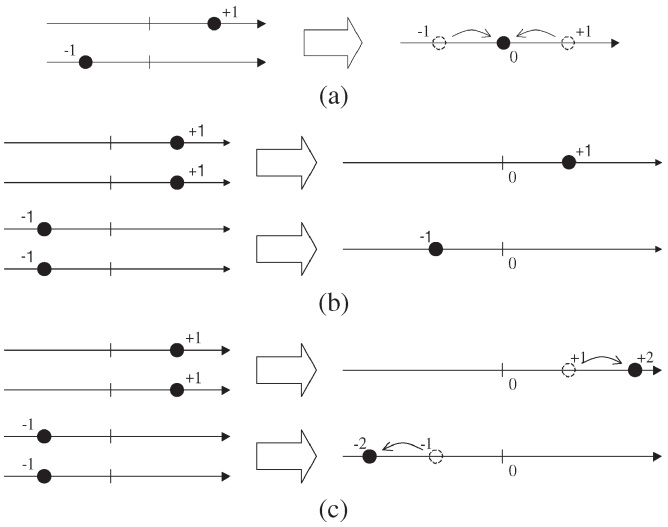

Fig. 1. Symbol mapping (BPSK). (a) Perforation. (b) Synergy with the amplitude of one symbol. (c) Synergy with the amplitude of two symbols.

The LLR is proportional to the receiving symbol amplitude y in additive white Gaussian noise (AWGN) channels. The channel demodulator output is then used as channel decoder input with channel reliability. Generally, under arbitrary symbol mapping, LLR can be approximated as the difference between the square of the closest Euclidean distances with symbols of 0 and 1 [11], [12].

$$L(y|d) \approx c \left[\min_{s_i \in S_1} \left\{ (y - s_i)^2 \right\} - \min_{s_i \in S_0} \left\{ (y - s_i)^2 \right\} \right] \tag{2}$$

where c is a constant related to channel reliability, and S_1 and S_0 are sets consisting of symbols having information of 1 and 0 in data modulation, respectively. The channel demodulator output is converted according to (2). These LLR calculations and conversions should be carefully examined in OCHM because perforation causes changes in symbol mapping.

When OCHM-based downlink experiences collisions among symbols during statistical multiplexing, the location of transmitted symbols can be different from the original locations in the $I-Q$ plane due to perforations. These locations are determined by data modulation and perforation schemes. Perforated symbols are generally placed at the origin of the plane in the case of BPSK/QPSK. LLR conversion schemes are proposed at the receiver according to changes in symbol mapping at the transmitter. LLR conversion improves performance by inserting a simple conversion (demapping) function between channel demodulator output and channel decoder input.

LLR is calculated differently according to symbol mapping in data modulation. Collision and perforation cause changes in OCHM symbol mapping. Perforation occurs when more than one symbol is transmitted on the same codeword (collision) and all symbol values are not identical. The simplest way to implement perforation is to map the colliding symbols to the origin of the plane in data modulation. Fig. 1(a) illustrates the perforation of data symbols to the origin for BPSK. If symbols on the same codeword are identical, we can choose the amplitude of one symbol, $|\pm 1|$ [Fig. 1(b)] or the amplitude of two symbols, $|\pm 2|$ [Fig. 1(c)] as the transmitted symbol. The latter slightly simplifies the system implementation. We propose LLR conversion methods to mitigate collisions for the cases shown in Fig. 1.

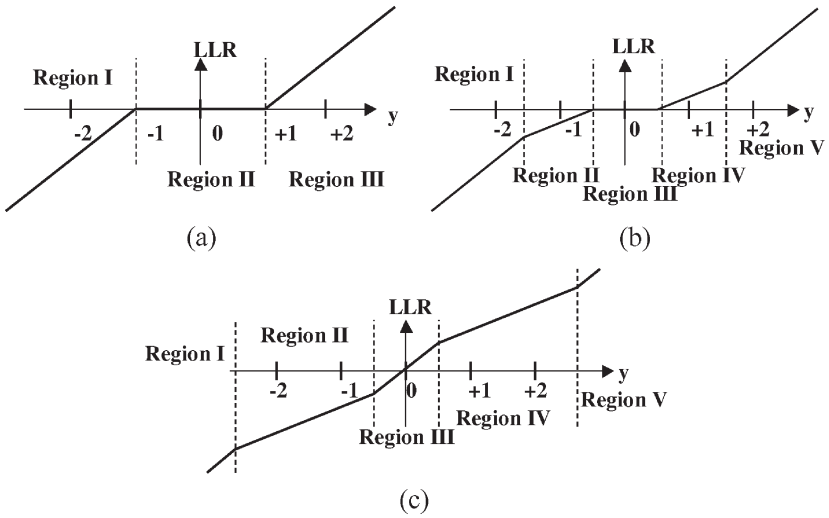

Fig. 2. Linear LLR conversion in case of considering both perforation and synergy. (a) Case 1. (b) Case 2. (c) Case 3.

A. Consideration of Perforation

When we transmit d and receive y, (1) is rewritten as (3) for equiprobable data symbols, considering only perforation

$$\begin{aligned} L(d|y) &= L(y|d) \\ &= \log \frac{(1-P_{\rm p})P(y|t=+1)+P_{\rm p}\cdot P(y|t=0)}{(1-P_{\rm p})P(y|t=-1)+P_{\rm p}\cdot P(y|t=0)} \\ &= \log \frac{(1-P_{\rm p})\exp\left(-\frac{(y-1)^2}{2\sigma^2}\right)+P_{\rm p}\exp\left(-\frac{y^2}{2\sigma^2}\right)}{(1-P_{\rm p})\exp\left(-\frac{(y+1)^2}{2\sigma^2}\right)+P_{\rm p}\exp\left(-\frac{y^2}{2\sigma^2}\right)} \end{aligned} \tag{3}$$

where t is the transmitted symbol, $P_{\rm p}$ is the perforation probability, and $\sigma^2=(1/2)(1/(E_{\rm s}/N_0))$ when considering perforation. This part was published in [13] and deals with Fig. 1(b) as synergy mapping. Therefore, we omit the procedures and results here. Fig. 1(a) is common and Fig. 1(c) is used in Section II-B.

B. Consideration of Both Perforation and Synergy

We now consider both perforation and synergy for symbol mapping [Fig. 1(c)]. The exact LLR conversion is expressed as (4), shown at the bottom of the page. $P_{\rm s}$ is the probability of synergy and is equal to $P_{\rm p}$ for two colliding users in (4). $P_{\rm s}$ is assumed to be equal to $P_{\rm p}$. Here, $P_{\rm p}$ is divided into three regions:

$$\begin{cases} \text{Case 1}: & P_{\rm p} > \frac{1}{2+\exp\left(-\frac{1}{2\sigma^2}\right)} \\ \text{Case 2}: & \frac{1}{2+\exp\left(\frac{1}{2\sigma^2}\right)} < P_{\rm p} \le \frac{1}{2+\exp\left(-\frac{1}{2\sigma^2}\right)} \\ \text{Case 3}: & P_{\rm p} \le \frac{1}{2+\exp\left(\frac{1}{2\sigma^2}\right)} \end{cases}. \tag{5}$$

The LLRs for the above three cases are approximated as (6)–(8), respectively

$$L(d|y) \approx \begin{cases} \frac{2}{\sigma^2}(y+1), & \text{Region I} \\ 0, & \text{Region II} \\ \frac{2}{\sigma^2}(y-1), & \text{Region III} \end{cases} \tag{6}$$

$$L(d|y) \approx \begin{cases} \frac{2}{\sigma^2}(y+1), & \text{Region I} \\ \log\frac{P_{\rm p}}{1-2P_{\rm p}}+\frac{1}{\sigma^2}\left(y+\frac{1}{2}\right), & \text{Region II} \\ 0, & \text{Region III} \\ \log\frac{1-2P_{\rm p}}{P_{\rm p}}+\frac{1}{\sigma^2}\left(y-\frac{1}{2}\right), & \text{Region IV} \\ \frac{2}{\sigma^2}(y-1), & \text{Region V} \end{cases} \tag{7}$$

$$L(d|y) \approx \begin{cases} \frac{2}{\sigma^2}(y+1), & \text{Region I} \\ \log\frac{P_{\rm p}}{1-2P_{\rm p}}+\frac{1}{\sigma^2}\left(y+\frac{1}{2}\right), & \text{Region II} \\ \frac{2y}{\sigma^2}, & \text{Region III} \\ \log\frac{1-2P_{\rm p}}{P_{\rm p}}+\frac{1}{\sigma^2}\left(y-\frac{1}{2}\right), & \text{Region IV} \\ \frac{2}{\sigma^2}(y-1), & \text{Region V} \end{cases}. \tag{8}$$

Fig. 2 shows these three conversion graphs. A high-perforation probability yields a broad erasure region around the origin in Fig. 2(a). As the perforation probability decreases, the erasure region shrinks and the region of the conventional slope expands around the origin in Fig. 2(c).

In summary, we propose an exact LLR conversion scheme and derive a piecewise linear LLR conversion scheme by approximation in order to reduce computational complexity. The piecewise linear conversion scheme exhibits a performance similar to the exact conversion scheme.

$$\begin{aligned} L(d|y) &= L(y|d) \\ &= \log \frac{(1-P_{\rm p}-P_{\rm s})P(y|t=+1)+P_{\rm p}\cdot P(y|t=0)+P_{\rm s}\cdot P(y|t=+2)}{(1-P_{\rm p}-P_{\rm s})P(y|t=-1)+P_{\rm p}\cdot P(y|t=0)+P_{\rm s}\cdot P(y|t=-2)} \\ &= \log \frac{(1-P_{\rm p}-P_{\rm s})\exp\left(-\frac{(y-1)^2}{2\sigma^2}\right)+P_{\rm p}\cdot\exp\left(-\frac{y^2}{2\sigma^2}\right)+P_{\rm s}\cdot\exp\left(-\frac{(y-2)^2}{2\sigma^2}\right)}{(1-P_{\rm p}-P_{\rm s})\exp\left(-\frac{(y+1)^2}{2\sigma^2}\right)+P_{\rm p}\cdot\exp\left(-\frac{y^2}{2\sigma^2}\right)+P_{\rm s}\cdot\exp\left(-\frac{(y+2)^2}{2\sigma^2}\right)} \end{aligned} \tag{4}$$

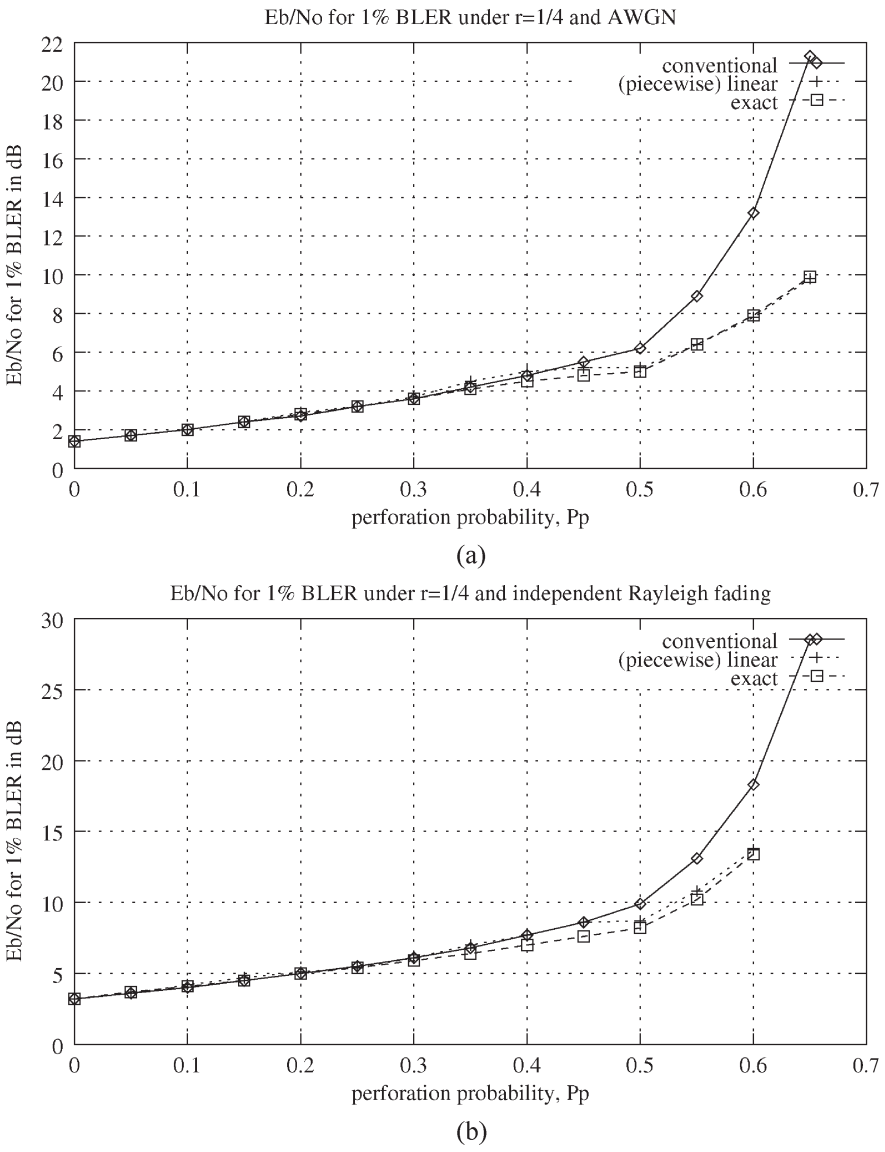

Fig. 3. Required $E_{\rm b}/N_0$ for a 1% BLER in case of considering both perforation and synergy. (a) AWGN channels. (b) Independent Rayleigh fading channels.

C. Numerical Results

Simulation environments are described assuming perfect channel estimation, phase equalization, and BPSK/QPSK. We first consider BPSK, however, simulation results can be applied to QPSK because QPSK can be characterized as two orthogonal BPSK channels [14]. Wireless channels are assumed to experience either AWGN or independent (uncorrelated) Rayleigh fading. No specific code-hopping patterns are designated and random hopping patterns are considered. Thus, symbol perforations occur randomly. Recursive systematic convolutional (RSC)-type parallel concatenated convolutional codes (PCCC), which are widely used in the third generation wireless communication systems [15], [16], are considered as an encoder. Turbo coding in third generation partnership project (3GPP) specifications is considered with the decoder using the soft output viterbi algorithm (SOVA) [17]. The number of decoding iterations is adaptive and is restricted to no more than 10. A 1% block error rate (BLER) [18] is assumed as a performance measure. The size of an encoder block is 1000 bits and the number of encoder blocks used in simulation is 10 000. The code rate r is 1/4.

Fig. 3 represents the required $E_{\rm b}/N_0$ value for a 1% BLER versus the perforation probability for the three LLR conversion schemes considering both perforation and synergy.[1] The two proposed schemes greatly reduce the required $E_{\rm b}/N_0$ value when the value of $P_{\rm p}$ is high. The proposed piecewise linear approximation scheme yields a similar performance to the exact scheme. Results for Sections II-A and II-B show a small difference in performance that can be used to determine which synergy strategy [Fig. 1(b) or (c)] is better. The result for Section II-B is better than that for Section II-A in this simulation. However, it is not true that the result of Fig. 1(c) indicates better performance than the Fig. 1(b) result. In other words, the optimum amplitude of a synergy symbol can be changed according to the code rate, channel codes, or decoding schemes. For example, the result of Fig. 1(b) is better than the Fig. 1(c) result when $r = 1/2$ and all other factors are the same. Determination of the optimum synergy amplitude is another topic that will require an exhaustive search.

[1]Results for Section II-A appeared in [13] and are omitted here.

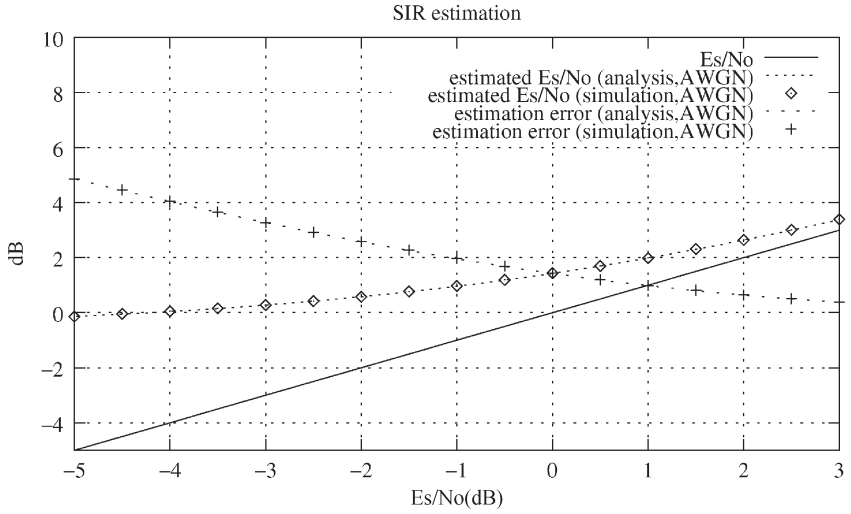

Fig. 4. SIR estimation (AWGN).

III. Estimation of the Perforation Probability

The perforation probability $P_{\rm p}$ must be estimated in advance in order to obtain an efficient LLR conversion. Estimation of the $P_{\rm p}$ value is required if there is no explicit knowledge of the value of $P_{\rm p}$ through signaling. We need to know the signal-to-interference ratio (SIR) to estimate the $P_{\rm p}$ value from the received symbols. This section starts with analysis of the SIR estimation, continues with the $P_{\rm p}$ estimation, and ends with numerical results.

A. SIR Estimation

The value of SIR can be estimated using the first and second moments [19], [20] when there is no perforation

$$\frac{E_{\rm s}}{N_0} = \frac{\mu^2}{2\sigma^2}$$
$$\hat{\mu} = \frac{1}{N}\sum_i |x_i|$$
$$\hat{\sigma^2} = \frac{1}{N}\sum_i |x_i|^2 - \hat{\mu}^2 \tag{9}$$

where x_is are the received symbols, N is the number of symbols, and μ and σ^2 represent the mean and variance of the received symbol amplitude, respectively. $\hat{\mu}$ and $\hat{\sigma^2}$ are the estimated values of μ and σ^2.

This method yields accurate results when the noise level is low. A $(+1)$ symbol transmission should yield a positive value reception. This will occur when the value of SIR is high. Fig. 4 compares SIR estimation results between analysis and simulation. A block for an SIR sample consists of 1000 symbols, and 1000 samples are obtained through simulation. Simulation results are in agreement with analytical results. When considering an $E_{\rm b}/N_0$ operating range from 2 to 10 dB in Fig. 3(a), the value of $E_{\rm s}/N_0$ varies from -4 to 4 dB for $r = 1/4$. The estimation error is then less than 4 dB in AWGN channels. The estimation error is severe in some regions. Thus, some compensation is required. The estimation error becomes larger for independent Rayleigh fading channels even for high values of $E_{\rm s}/N_0$. Estimating the value of SIR is a difficult problem for engineers designing mobile terminals.

B. Perforation Probability Estimation Methods

The receiver requires the value of $P_{\rm p}$ in advance for an efficient LLR conversion. Four estimation methods are proposed to obtain $P_{\rm p}$ information:

1) explicit notification through signaling;
2) zone detection;
3) an unbiased estimator of the first moment;
4) an unbiased estimator of the second moment.

The most reliable scheme is to explicitly send the information by signaling. However, this causes an increase in the signaling load.

A zone detection scheme is used to set a threshold around the origin and to count the number of perforated symbols in the region. The threshold value can be set to 0.5 when we have no information about perforation probability that determines the number of symbols around the origin. The $P_{\rm p}$ value can be estimated as (10) when $P_{\rm th}$ denotes the threshold

$$\begin{aligned}\hat{P}_{\rm ppre} &= P_{\rm p}\int_{-P_{\rm th}}^{P_{\rm th}} \frac{1}{\sqrt{2\pi}\sigma}{\rm e}^{-\frac{x^2}{2\sigma^2}}dx + (1-P_{\rm p}) \\ &\quad\times \int_{-P_{\rm th}}^{P_{\rm th}} \frac{1}{\sqrt{2\pi}\sigma}{\rm e}^{-\frac{(x-1)^2}{2\sigma^2}}dx \\ &= P_{\rm p} - 2P_{\rm p}Q\left(\frac{P_{\rm th}}{\sigma}\right) + (1-P_{\rm p}) \\ &\quad\times\left\{Q\left(\frac{1-P_{\rm th}}{\sigma}\right) - Q\left(\frac{1+P_{\rm th}}{\sigma}\right)\right\}. \end{aligned} \tag{10}$$

$\hat{P}_{\rm ppre}$ is the estimated probability of the number of symbols around the origin. Equation (10) has an estimation offset in the tail of the equation. Thus, it can be rewritten as

$$\begin{aligned}\hat{P}_{\rm ppre} &= \left\{1 - 2Q\left(\frac{P_{\rm th}}{\sigma}\right) - Q\left(\frac{1-P_{\rm th}}{\sigma}\right) + Q\left(\frac{1+P_{\rm th}}{\sigma}\right)\right\}P_{\rm p} \\ &\quad + \left\{Q\left(\frac{1-P_{\rm th}}{\sigma}\right) - Q\left(\frac{1+P_{\rm th}}{\sigma}\right)\right\} \\ &= A(\sigma, P_{\rm th})P_{\rm p} + B(\sigma, P_{\rm th}). \end{aligned} \tag{11}$$

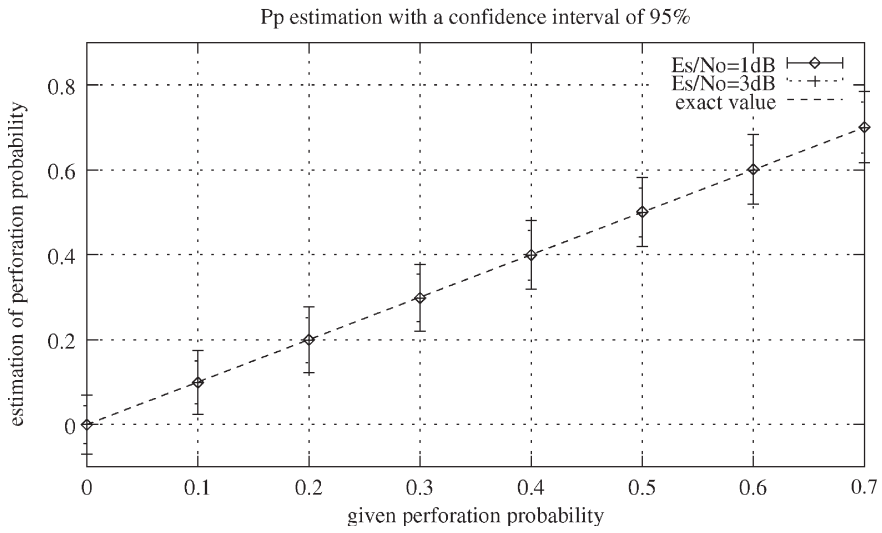

Fig. 5. Estimated perforation probability with a confidence interval of 95% with a known SIR.

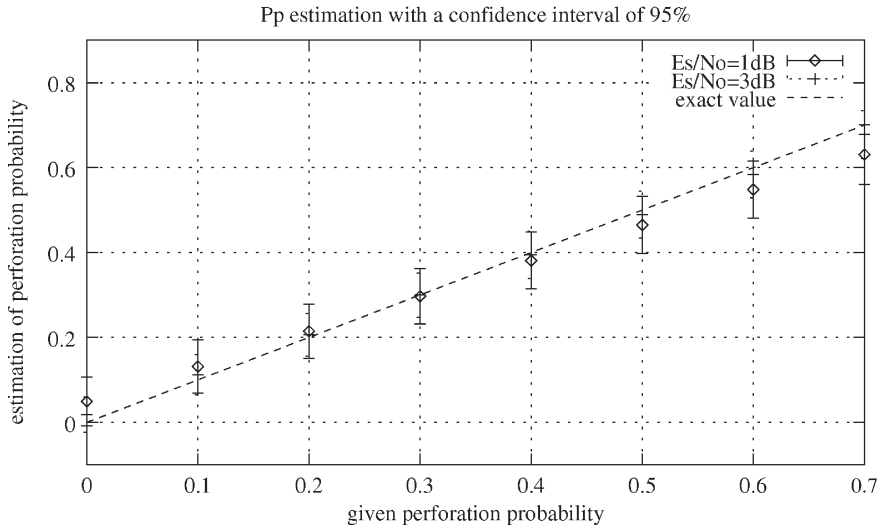

Fig. 6. Estimated perforation probability with a confidence interval of 95% with SIR estimation.

Then, the unbiased estimator is expressed as

$$\hat{P}_{\mathrm{p}} = \frac{\hat{P}_{\mathrm{ppre}} - B(\sigma, P_{\mathrm{th}})}{A(\sigma, P_{\mathrm{th}})}. \tag{12}$$

Finally, estimation schemes based on moments are used to calculate the first and second moments for the received symbols and to estimate the value of P_{p}. The first and second moments are obtained as

$$\begin{aligned} E\left[|X|\right] &= P_{\mathrm{p}} \int_{-\infty}^{\infty} |x| \frac{1}{\sqrt{2\pi}\sigma} \mathrm{e}^{-\frac{x^2}{2\sigma^2}} dx + (1 - P_{\mathrm{p}}) \\ &\quad \times \int_{-\infty}^{\infty} |x| \frac{1}{\sqrt{2\pi}\sigma} \mathrm{e}^{-\frac{(x-1)^2}{2\sigma^2}} dx \\ &= \left\{ 2Q\left(\frac{1}{\sigma}\right) - 1 + \sqrt{\frac{2}{\pi}}\sigma\left(1 - \mathrm{e}^{-\frac{1}{2\sigma^2}}\right) \right\} P_{\mathrm{p}} \\ &\quad + \left\{ 1 - 2Q\left(\frac{1}{\sigma}\right) + \sqrt{\frac{2}{\pi}}\sigma \mathrm{e}^{-\frac{1}{2\sigma^2}} \right\} \\ &= C(\sigma) P_{\mathrm{p}} + D(\sigma) \end{aligned} \tag{13}$$

$$\begin{aligned} E[X^2] &= P_{\mathrm{p}} \int_{-\infty}^{\infty} x^2 \frac{1}{\sqrt{2\pi}\sigma} \mathrm{e}^{-\frac{x^2}{2\sigma^2}} dx + (1 - P_{\mathrm{p}}) \\ &\quad \times \int_{-\infty}^{\infty} x^2 \frac{1}{\sqrt{2\pi}\sigma} \mathrm{e}^{-\frac{(x-1)^2}{2\sigma^2}} dx \\ &= \sigma^2 + 1 - P_{\mathrm{p}}. \end{aligned} \tag{14}$$

X is the random variable representing the received symbol amplitude.

$E[|X|]$ and $E[X^2]$ are first-order equations of P_{p}. Therefore, an unbiased estimate of the value of P_{p} can be obtained as the first-order equation of $E[|X|]$ or $E[X^2]$

$$\begin{aligned} \hat{P}_{\mathrm{p}} &= \frac{E\left[|X|\right] - D(\sigma)}{C(\sigma)} \\ &= 1 + \sigma^2 - E[X^2]. \end{aligned} \tag{15}$$

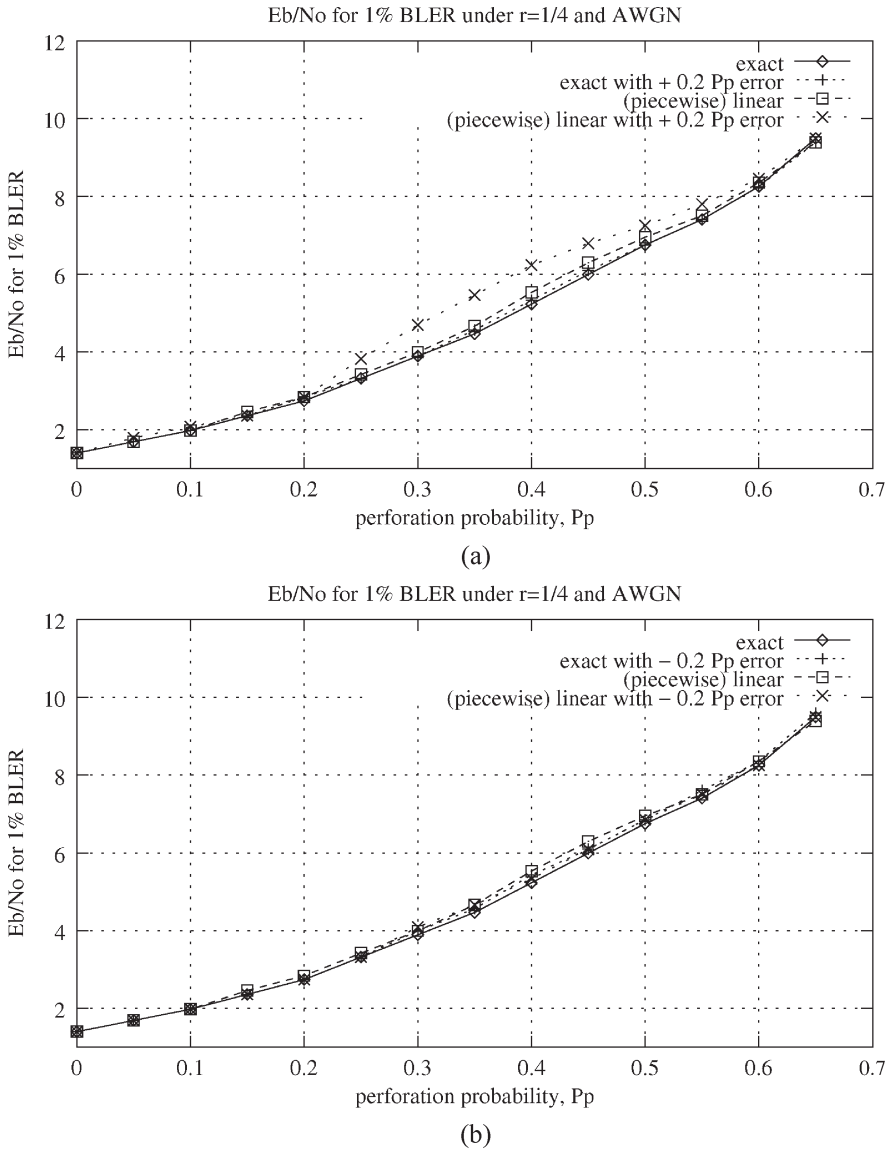

Fig. 7. Required $E_{\rm b}/N_0$ for a 1% BLER when $P_{\rm p}$ estimation error is ± 0.2. (a) $+0.2$ $P_{\rm p}$ error. (b) -0.2 $P_{\rm p}$ error.

C. Simulation With a Known Value of SIR

Simulation procedures are described as follows:

1) estimation of the $P_{\rm p}$ value from a block size of 1000;
2) iterations of 1000 blocks;
3) calculation of the sample mean and the sample variance;
4) derivation of the confidence interval for samples to be obtained.

The value of $P_{\rm p}$ is estimated from 1000 symbols. Therefore, the $P_{\rm p}$ value follows a Gaussian distribution according to the central limit theorem [21]. Let 1000 $P_{\rm p}$s be $P_{{\rm p},1}, P_{{\rm p},2}, \ldots, P_{{\rm p},1000}$ with a sample mean of $\bar{P}_{\rm p}$ and a sample variance of s^2. Then, $\bar{P}_{\rm p}$ and s^2 are obtained as

$$\bar{P}_{\rm p} = \frac{1}{N}(P_{{\rm p},1} + P_{{\rm p},2} + \cdots + P_{{\rm p},N})$$
$$s^2 = \frac{1}{N-1}\sum_i (P_{{\rm p},i} - \bar{P}_{\rm p})^2 \tag{16}$$

where $N = 1000$. Assuming that the estimated mean and variance of the Gaussian distribution are correct, we show the interval in which a $P_{\rm p}$ value is obtained at the proper significance level [21]

$$\left(\bar{P}_{\rm p} - z_{\frac{\alpha}{2}}\, s, \bar{P}_{\rm p} + z_{\frac{\alpha}{2}}\, s\right) \tag{17}$$

where $(1-\alpha)$ is the desired probability and $z_{\alpha/2}$ is a point on the standard normalized z axis.

The above procedures allow simulation of the $P_{\rm p}$ estimation when the SIR value is known. Results are based on the zone detection scheme. The estimated perforation probability with a confidence interval of 95% is shown in Fig. 5. Deviation from a given value of $P_{\rm p}$ is less than 0.084 for $E_{\rm s}/N_0 = 1$ dB, and 0.060 for $E_{\rm s}/N_0 = 3$ dB, where $E_{\rm s}/N_0$ is the value before perforation.

D. Simulation With SIR Estimation

Simulation is executed after SIR estimation of Section III-A. Performance is expected to be degraded due to SIR estimation error. Fig. 6

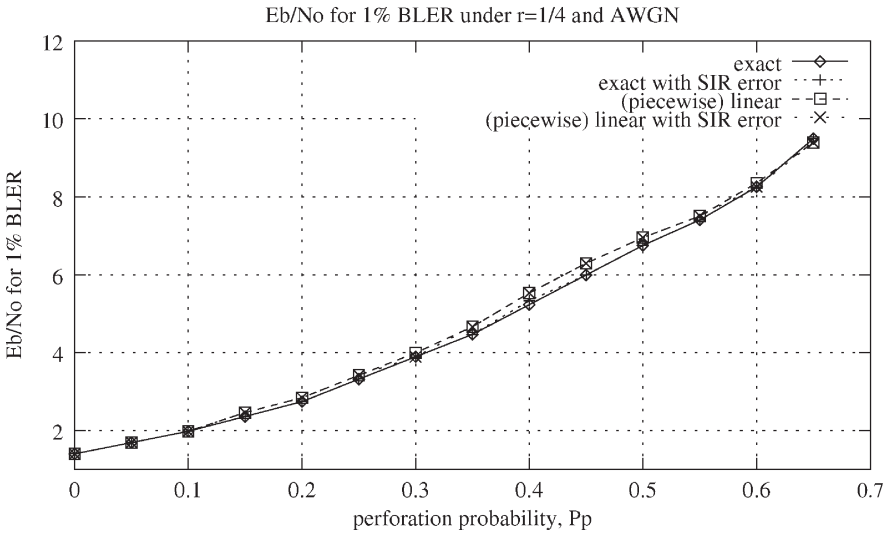

Fig. 8. Required E_{b}/N_0 for a 1% BLER when P_{p} estimation error is induced by SIR estimation error.

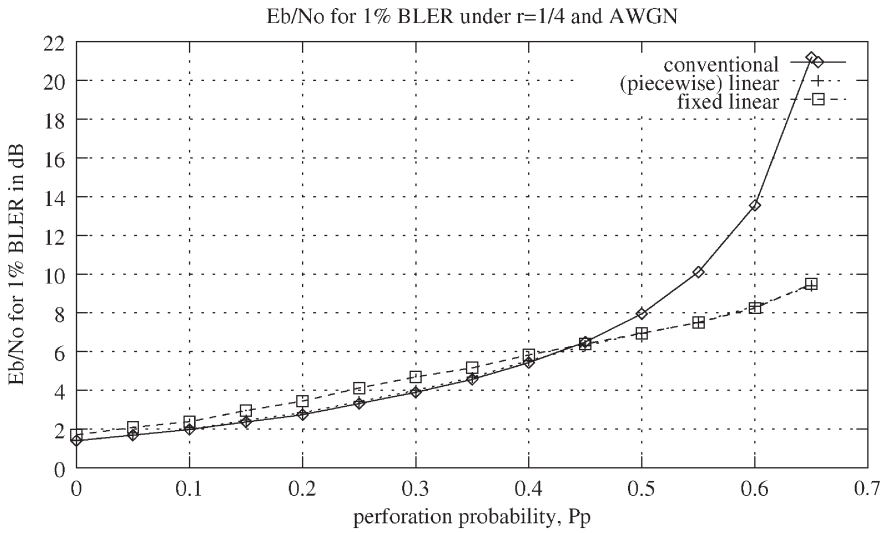

(a)

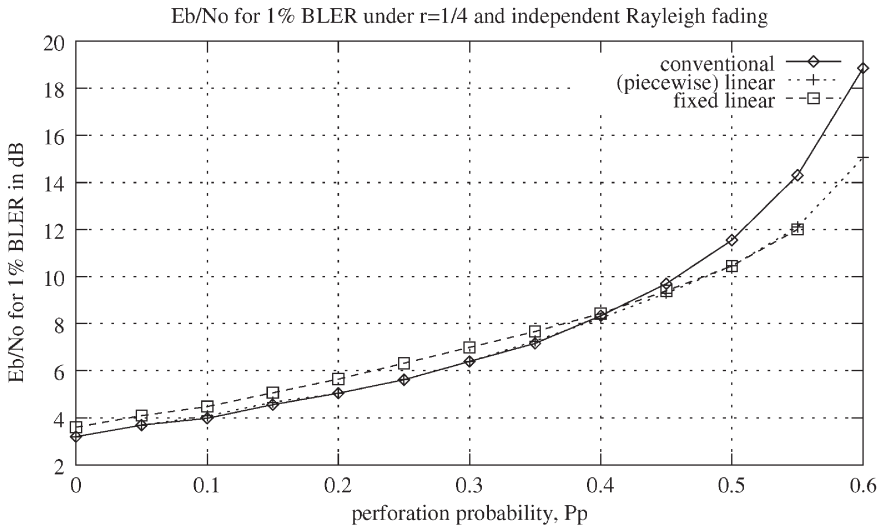

(b)

Fig. 9. Required E_{b}/N_0 of the fixed linear scheme for a 1% BLER in case of considering perforation. (a) AWGN channels. (b) Independent Rayleigh fading channels.

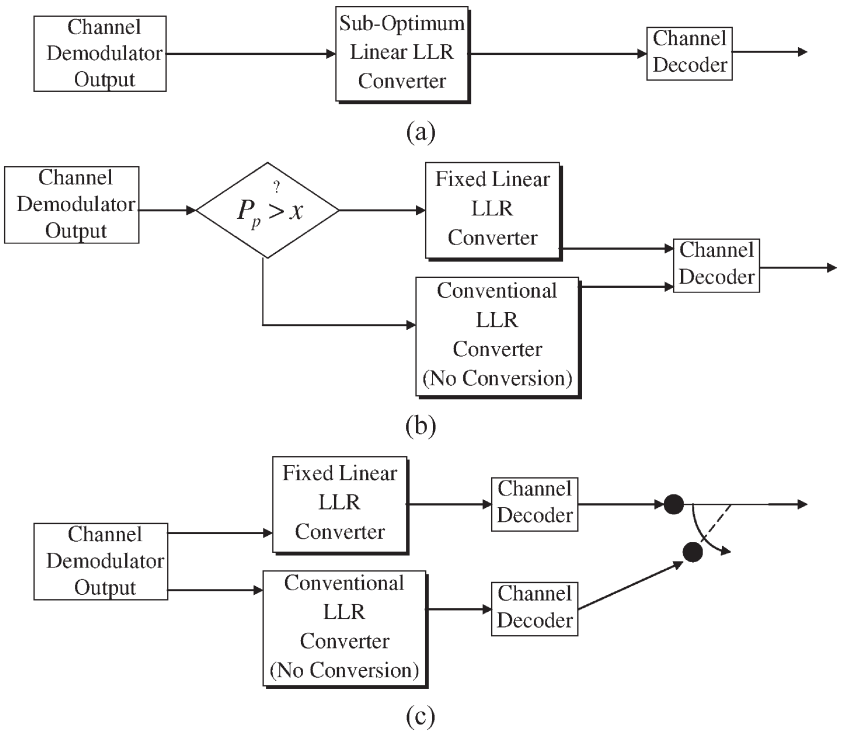

Fig. 10. LLR conversion schemes adopting the fixed linear scheme. (a) (Piecewise) Linear scheme. (b) Switching scheme from perforation probability. (c) Switching scheme from parallel decoding.

illustrates the estimation of P_{p} obtained with a confidence interval of 95%. Deviation from a given value of P_{p} is less than 0.139 for $E_{\mathrm{s}}/N_0 = 1$ dB, and 0.079 for $E_{\mathrm{s}}/N_0 = 3$ dB.

E. Simulation With Perforation Probability Estimation Error

This part investigates how false information on perforation probability affects the BLER performance. Simulation results are provided for the situation that the system operates with a false P_{p} but the actual P_{p} is something different. First, we assume ± 0.2 estimation error for P_{p}. Fig. 7 illustrates the required E_{b}/N_0 deviation for a 1% BLER. In Fig. 7(a), the deviation for the exact scheme is small, but the linear scheme deviates by 0.8 dB in some region. On the other hand, Fig. 7(b) shows that the deviation is small within 0.2 dB. This simply indicates that overestimation is likely to be worse than underestimation. A biased estimator for P_{p} toward low values is more likely to be useful for the system.

In spite of Fig. 7, Fig. 8 shows that P_{p} estimation error has little impact on performance. Perforation probability estimation error is induced by SIR estimation error of Section III-A. P_{p} error is a function of the actual P_{p} and SIR error. Therefore, the curves of Fig. 8 are obtained under P_{p} error calculated by SIR estimation error. In fact, P_{p} errors of ± 0.2 are large, and the SIR estimation error does not yield such a large P_{p} error. E_{b}/N_0 deviation in Fig. 8 lies only within 0.1 dB. Fig. 7 illustrates the effect of large P_{p} errors in both directions. We conclude that perforation probability estimation error induced by SIR estimation error has little impact on performance.

IV. Fixed Linear LLR Conversion

In the previous section, we observed that a small error for the perforation probability estimation has little impact on performance. Since the new schemes exhibit large performance improvements for high P_{p} values, we select a representative fixed conversion graph from curves of high P_{p} values and observe its performance. We obtain it at the point that the conversion graph changes its total shape into those of high P_{p} region and call it a fixed linear conversion scheme

$$L(d|y) \approx \begin{cases} \frac{1}{\sigma^2}\left(y+\frac{1}{2}\right), & \text{Region I} \\ 0, & \text{Region II} \\ \frac{1}{\sigma^2}\left(y-\frac{1}{2}\right), & \text{Region III} \end{cases}. \tag{18}$$

The fixed liner scheme is expressed as (19) for LLR conversion with consideration of both perforation and synergy

$$L(d|y) \approx \begin{cases} \frac{2}{\sigma^2}(y+1), & \text{Region I} \\ \frac{1}{\sigma^2}\left(y+\frac{1}{2}\right), & \text{Region II} \\ 0, & \text{Region III} \\ \frac{1}{\sigma^2}\left(y-\frac{1}{2}\right), & \text{Region IV} \\ \frac{2}{\sigma^2}(y-1), & \text{Region V} \end{cases}. \tag{19}$$

We can obtain a much simpler LLR conversion using the fixed linear conversion scheme with acceptance of a slight degradation in performance. Fig. 9 shows a comparison of 1) the conventional scheme (without conversion), 2) the (suboptimum) linear scheme, and 3) the fixed linear scheme using (18). It is natural that the (suboptimum) linear conversion scheme always yields good performance but it also requires some estimation of the P_{p} value. The conventional and the fixed linear schemes do not require any estimation of the P_{p} value. From Fig. 9, combination of the conventional and fixed linear schemes yields a performance similar to the (suboptimum) linear scheme. The difference in the value of E_{b}/N_0 between the linear scheme and the combination of the other two schemes is negligible, occurring at a P_{p} value of approximately 0.4. Results for (19) considering both perforation and synergy show a trend similar to that seen in Fig. 9.

When we adopt a combination of the conventional and the fixed linear schemes instead of the (suboptimum) linear scheme, two choices are possible, as depicted in the last two subfigures of Fig. 10. We had better adopt a better region of each scheme. The first choice of Fig. 10(b) is to use either the conventional or the fixed linear scheme

after a rough estimation of the value of P_{p} since two curves of the conventional scheme and the fixed linear one meet only once around P_{p} of 0.4. We need to determine whether or not the value of P_{p} is greater than 0.4. The second choice of Fig. 10(c) is to select one result after two parallel decoding processes of the conventional scheme and the fixed linear scheme. We will choose either decoding output without block error notification such as cyclic redundancy check (CRC) error. This would require more power due to parallel decoding but no estimation of the P_{p} value.

V. Conclusion

An OCHM scheme [1], [2] has been proposed as a novel statistical-multiplexing scheme for orthogonal downlink to accommodate more low-activity bursty users than the number of orthogonal downlink codewords. OCHM can cause perforations among symbols, which degrade the performance of channel decoding when the perforation probability is high. We propose new LLR conversion schemes that improve the decoding performance in perforation environments. The schemes require a simple conversion function between channel demodulator output and channel decoder input. We propose several types of LLR conversion functions. The proposed schemes reduce the required E_{b}/N_0 value by up to 10 dB when the value of P_{p} is high. The piecewise linear (suboptimum) conversion scheme yields performance similar to the exact (optimum) scheme and reduces computational complexity. In these LLR conversion schemes, estimation of the perforation probability is required. Therefore, several estimation methods are proposed. The fixed linear LLR conversion scheme without estimation of the perforation probability is proposed to avoid accurate estimation. Combination of the conventional and fixed linear conversion schemes does not require an exact estimation of the perforation probability. However, performance is similar to the (suboptimum) linear conversion scheme.

References

[1] S. Park and D. K. Sung, "Orthogonal code hopping multiplexing," *IEEE Commun. Lett.*, vol. 6, no. 12, pp. 529–531, Dec. 2002.

[2] ——, "Orthogonal code hopping multiplexing for downlink in spread communication," in *Proc. Multi-Dimensional Mobile Communication Conf. (MDMC)*, Pori, Finland, Jun. 2001, pp. 365–372.

[3] J. K. Kwon, S. Park, D. K. Sung, and M. G. Kyeong, "Performance comparison of orthogonal code hopping multiplexing (OCHM) and HDR schemes in synchronous downlink," in *Proc. Wireless Communications and Networking Conf. (WCNC)*, Orlando, FL, Mar. 2002, pp. 200–205.

[4] J. K. Kwon, S. Park, D. K. Sung, and H. Lee, "Adaptive code rate for orthogonal code hopping multiplexing (OCHM) in synchronous downlink," in *Proc. Wireless Communications and Networking Conf. (WCNC)*, New Orleans, LA, Mar. 2003, pp. 855–859.

[5] S. Park, S. H. Moon, J. K. Kwon, and D. K. Sung, "Orthogonal code hopping multiplexing for downlink statistical multiplexing," in *Proc. Int. Symp. Spread Spectrum Techniques and Applications (ISSSTA)*, Prague, Czech Republic, Sep. 2002, pp. 588–592.

[6] T. Onizawa and T. Hasegawa, "The spread spectrum code hopping system," in *Proc. Int. Symp. Spread Spectrum Techniques and Applications (ISSSTA)*, Oulu, Finland, Jul. 1994, pp. 287–291.

[7] B. Unal and Y. Tanik, "Code-hopping as a new strategy to improve performance of S-CDMA cellular systems," in *Proc. Global Telecommunications (GLOBECOM)*, London, U.K., Nov. 1996, pp. 1316–1319.

[8] ——, "Capacity improvement by code-hopping in S-CDMA systems," in *Proc. Int. Conf. Communications (ICC)*, Atlanta, GA, Jun. 1998, pp. 989–993.

[9] I. G. Kim, K. Kim, and B. W. Lim, "A fast cell search algorithm for inter-cell asynchronous W-CDMA system using code hopping method," in *Proc. Global Telecommunications (GLOBECOM)*, Sydney, Australia, Nov. 1998, pp. 1373–1377.

[10] B. Sklar, "A primer on turbo code concepts," *IEEE Commun. Mag.*, vol. 35, no. 12, pp. 94–101, Dec. 1997.

[11] B. Vucetic and J. Yuan, *Turbo Codes: Principles and Applications*. Norwell, MA: Kluwer, 2000.

[12] 3GPP, *3rd Generation Partnership Project: Technical Specification Group Radio Access Network; Physical Layer Aspects of UTRA High Speed Downlink Packet Access*, Mar. 2001. 3GPP TR25.848 V4.0.0.

[13] J. K. Kwon, S. Park, and D. K. Sung, "Log-likelihood ratio (LLR) conversion schemes in orthogonal code hopping multiplexing," *IEEE Commun. Lett.*, vol. 7, no. 3, pp. 104–106, Mar. 2003.

[14] B. Sklar, *Digital Communications: Fundamentals and Applications*. Upper Saddle River, NJ: Prentice-Hall, 1988.

[15] 3GPP, *3rd Generation Partnership Project: Technical Specification Group Radio Access Network*, 2001. 3GPP TS 25 series.

[16] 3GPP2, *cdma2000 High Rate Packet Data Air Interface Specification: Version 2.0*, Oct. 2000.

[17] J. P. Woodard and L. Hanzo, "Comparative study of turbo decoding techniques: An overview," *IEEE Trans. Veh. Technol.*, vol. 49, no. 6, pp. 2208–2233, Nov. 2000.

[18] Qualcomm, *1xHDR: 1x Evolution (1xEV) Airlink Overview*, Aug. 2000.

[19] S. Gunaratne, S. Nourizadeh, T. Jeans, and R. Tafazolli, "Performance of SIR-based power control for UMTS," in *Proc. 2nd Int. Conf. 3G Mobile Communication Technologies*, London, U.K., Mar. 2001, pp. 16–20.

[20] S. Gunaratne, P. Taaghol, and R. Tafazolli, "Signal quality estimation algorithm," *Electron. Lett.*, vol. 36, no. 22, pp. 1882–1884, Oct. 2000.

[21] E. R. Dougherty, *Probability and Statistics for the Engineering, Computing and Physical Sciences*. Upper Saddle River, NJ: Prentice-Hall, 1990.

Limited Feedback Diversity Techniques for Correlated Channels

David J. Love and Robert W. Heath, Jr.

***Abstract*—Employing multiple antennas at the transmitter is a well-established technique for providing diversity advantage in wireless systems. Transmit beamforming relies on the assumption of current channel knowledge at the transmitter, which is unrealistic when the forward and reverse links are separated in frequency. One solution to this problem is for the receiver to send a small number of feedback bits that convey channel information to the transmitter. Feedback design techniques have been proposed over the past few years, but they were derived using the assumption of spatially uncorrelated Rayleigh fading. This correspondence addresses the design of limited feedback beamformers when the channel is correlated.**

***Index Terms*—Beamforming, diversity methods, limited feedback, multiple antennas.**

I. Introduction

Multiantenna transmitters can provide reduced error rates and increased capacities by mitigating the effects of multipath fading caused by the channel. Closed-loop techniques obtain these benefits by adapting the transmitted signal using forward-link channel knowledge.

Manuscript received August 11, 2004; revised December 21, 2004 and September 27, 2005. This work was supported in part by the Office of Naval Research under Grant N00014-05-1-0169, the SBC Foundation, and the National Science Foundation (NSF) under Grants CCF-0513916 and CCF-0514194. This correspondence was presented in part at the IEEE Global Telecommunications Conference, Dallas, TX, November–December 2004. The review of this paper was coordinated by Dr. E. Larsson.

D. J. Love is with the School of Electrical and Computer Engineering, Purdue University, West Lafayette, IN 47907 USA (e-mail: djlove@ecn.purdue.edu).

R. W. Heath, Jr. is with the Department of Electrical and Computer Engineering, The University of Texas at Austin, Austin, TX 78712 USA (e-mail: rheath@ece.utexas.edu).

Digital Object Identifier 10.1109/TVT.2005.863346